Sādhanā (2026) 51:377
https://doi.org/10.1007/s12046-026-03330-2

Optimising natural frequencies of functionally graded beams via CPA and TWO metaheuristic algorithms

MAJED KANOUA[1,*], AHMAD RESHAD NOORI[1] and
MARWAN ABDULKAREEM SHAKIR ALBAYATI[2]

[1]Department of Civil Engineering, Istanbul Gelisim University, Istanbul, Turkey
[2]Esenyurt, Istanbul, Türkiye
*Corresponding Author. E-mail: marwanshakir6@gmail.com

MS received 10 September 2025; revised 25 March 2026; accepted 7 June 2026
© The Author(s), under exclusive licence to Indian Academy of Sciences 2026

Abstract. This research aims to optimise the lowest natural frequencies of functionally graded beams using the power-law distribution under classical boundary conditions (simply supported, clamped–clamped, and clamped–free) through material gradation across the beam thickness. To include the effect of mechanical properties gradient, the classical Euler–Bernoulli beam theory is expanded, which leads to a local change in mass density and stiffness modulus. The solution is achieved using two modern metaheuristic algorithms. This study investigates the application of metaheuristic algorithms for optimising the dynamic behaviour of functionally graded beams under classical boundary conditions. The two algorithms used are Tug of War optimisation algorithm (TWO), and Cyclical Parthenogenesis algorithm (CPA) to overcome the traditional constraints by using adaptive penalty functions to impose mass and manufacturability constraints, because the highly non-convex and nonlinear design space. The results show that the CPA algorithm provides high-quality solutions by achieving rapid convergence, making it suitable for time- and mass-sensitive designs. The TWO algorithm, on the other hand, offer greater improvement in natural frequency of up to 25%, but with a longer processing time therefore it is suitable when vibration efficiency is a priority. This research highlights the potential of intelligent algorithms in the design of high-performance composite beams and contributes to laying the foundation for future expansion of the study to 3D panels and shells using 3D printing.

Keywords. Functionally graded beams; natural frequency optimisation; Tug of War optimisation algorithm; Cyclical Parthenogenesis algorithm; Euler–Bernoulli beam theory.

1. Introduction

Functionally graded materials (FGMs) have emerged as an advanced class of composite materials characterised by the continuous variation of material properties, offering superior mechanical and thermal performance compared with conventional homogeneous materials. A specified function (such as a power-law, exponential, or sigmoid function) controls the variation of the local volume fractions of the component materials in these beams, which are often a combination of metals, ceramics, or polymers. Due to this gradation, the thickness of the beam causes a proportional change in characteristics, including density, thermal expansion coefficient, and Young's modulus *E*. Usually, the analysis of FGM beams is based on traditional beam theories like Timoshenko or Euler–Bernoulli beam theory. The stiffness and other material properties are no longer constant but rather functions of the spatial coordinate (typically indicated by the thickness direction) in these models, which assume that the displacement fields are functions of the beam's shape and loading. For instance, the Young's modulus follows a power-law distribution as it changes over the thickness z.

FGM beams have a great appeal due to their ability to distribute stresses more evenly, as shown in figure 1. This reduces areas of high stress, increases resistance to high temperatures, improves mass distribution and stiffness by improving vibration characteristics and increases damage tolerance [1]. This paper presents a comprehensive review of the existing literature on FGMs, highlighting recent advances, key challenges, and future research directions [2]. The free vibration characteristics, i.e., the natural frequencies and associated mode shapes, are affected by the gradation index and the specific variation of material quality [3].

A mathematical analytical model of the free vibrations of a functionally graded beam (FGB) is developed by increasing the beam thickness, providing closed-form solutions for accurate prediction of natural frequencies and mode shapes [4]. The vibrational behaviour of FGB

Published online: 12 October 2026

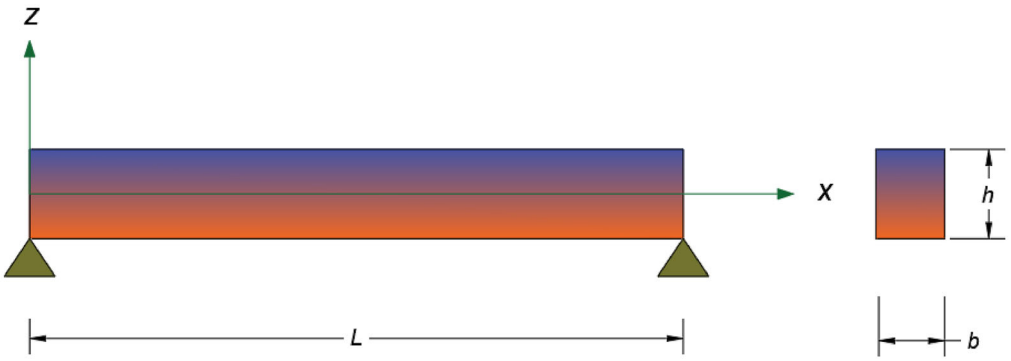


Figure 1. Schematic representation of a functionally graded beam.

subjected to a moving mass is investigated. It evaluated how material gradation and the moving load affected the beam's vibrations and compared various beam theories to see how well they predict the dynamic response [5]. An extensive mathematical structure to examine the behaviour of functionally graded porous beams when significant deflection is created. They looked into how material gradation and porosity distributions affected structural performance, offering guidance for the development and improvement of such cutting-edge materials for engineering applications [6]. An effective numerical process to examine the dynamic response of functionally graded porous (FGP) beams and the CFM in the Lapglace domain to solve the governing equations of motion for FGP beams is used [7]. The static behaviour of FGP planar frames is investigated using a precise and efficient numerical method based on CFM to solve the governing equilibrium equations. [8]. A higher-order shear deformation beam theory is employed, taking into account the bidirectional distributions of material properties, including density, Poisson's ratio, and Young's modulus, each of which is modelled using a power-law index along the thickness and width of the beam [9]. The structural response of these panels under different loading conditions is examined to optimise the factors affecting their bending characteristics [10]. Different higher-order shear deformation beam theories are employed to investigate the bending and free vibration behaviours of FGB by considering the variation of transverse shear strain through the beam thickness and the stress on the above and below surfaces [11]. A new frequency solution for FGB and some mode shapes is found by using the differential transformation method for different limit conditions and material gradations [12]. The natural frequencies of axially FGBs and arches are improved by tailoring the longitudinal material distribution. The fundamental vibration characteristics are optimised by modifying the parameters of four- and five-parameter volume fraction functions. [13].

The natural frequency properties of curved FGBs with porosity is examined. A higher-order shear deformation theory, three-node finite elements, and first-order perturbation techniques are employed [14]. A finite element analysis of the free vibration characteristics of two-dimensional functionally graded (2D-FG) strip beams with material stiffness and density that vary continuously in both axial and thickness directions is performed using the Voigt rule of mixtures and power-law gradation. A modal analysis and plane-stress formulation using ANSYS was also performed [15]. The dynamic behaviour of the beams is investigated by considering various material distributions, slenderness ratios, and boundary conditions. The results are presented both graphically and in tabular form to provide a comprehensive understanding of the factors influencing the free vibration characteristics of FGMs [16]. A range of optimisation techniques, such as gradient-based, metaheuristic, and hybrid approaches is used, to improve FGM performance in structural applications [17]. The free vibration characteristics are examined by modelling the beams using the finite element approach, taking into account the effects of rotary inertia and transverse shear deformation [18]. The dynamic response of the beam structure is analysed by investigating the effects of porosity parameters, material gradation, and boundary conditions. A nonlinear formulation is developed using Reddy beam theory and von Kármán geometric nonlinearity [19]. The free vibration properties of FGBs is examined by using the Euler–Bernoulli and Timoshenko beam theories. Using the Rayleigh–Ritz approach to obtain approximate solutions, the natural frequencies are determined for different material gradations and boundary conditions [20]. The transverse bending and semi-inverse behaviour of beams with specific cross-sectional shapes are analysed by combining two governing equations into a single equation for deflection and the angle of rotation [21]. A fourth-order governing equation for FGM beams is analysed. The equation accounts for variations in the elasticity modulus and mass density arising from changes in the material properties and volume fraction distribution. A finite element method is developed by using exact form functions to study an axially functionally graded tapered Timoshenko beam, improving

the material characteristics and cross-sectional profile [22]. The exact frequency equations for free vibration are developed by considering the exponential variation of material properties along the beam length [23]. The bending and free vibration characteristics of FGBs are analysed using the Euler–Bernoulli beam theory. The study aims to investigate the effect of the power-law gradient index on the displacements and natural frequencies and to validate the proposed methodology through close agreement between the analytical, computational, and experimental results. [24].

Metaheuristic algorithms are of great importance in structural engineering, as they are widely used to solve complex, multi-objective, non-linear problems. They have been applied in various fields, including the design of castellated beams, the calculation of vertical displacements, and the design of axisymmetric cylindrical walls. Therefore, algorithms contribute to effective solutions for a wide range of engineering applications [25–47].

Despite the extensive studies on the vibration analysis of FGBs, the systematic optimisation of dynamic performance under practical design constraints remains relatively underexplored. Prior works emphasise on analytical or numerical modelling and parametric sensitivity, but fewer studies investigate on how different metaheuristic search philosophies influence optimal design configurations and convergence behaviour under identical boundary conditions and constraints, mainly due to the high nonlinearity of the design space and the computational cost associated with ensuring fair and consistent algorithmic comparison. The present study addresses this gap by introducing a unified optimisation framework that integrates two conceptually different metaheuristic algorithms (CPA and TWO) to enhance the natural frequencies of FGBs under classical boundary conditions. The framework simultaneously optimises cross-sectional dimensions and the material gradation index under consistent constraints, enabling a structured comparison of algorithmic behaviour, convergence characteristics, and resulting design tendencies. The findings provide practical guidance for selecting suitable optimisation strategies based on design priorities, such as rapid convergence, solution feasibility, or maximum vibration performance.

2. Methodology

2.1 *Overview of the optimisation framework*

In this study, a custom MATLAB script is developed to perform structural optimisation of a FGB by integrating the TWO and CPA methods. The code is written entirely in MATLAB version 2024 and relies on vectorised operations and built-in functions from the Optimisation Toolbox to evaluate natural frequencies and enforce geometric and material constraints via a quadratic penalty function. TWO is implemented with adaptive wave amplitude control, while CPA is encapsulated, using inertia weight updates and velocity clamping to maintain feasibility. Both routines accept the same input structures, including design variables, bounds, penalty weights, and return the optimal design vectors together with their convergence histories. There are 4 categories of beams, 5 iterations, and 3 boundary conditions. 60 examples for each method is solved accordingly to different iterations and codes. Iterations of 10, 20, 30, 40, and 50 are used to evaluate the performance differences, with the method demonstrating superior performance during the early iterations. Therefore, both codes TWO and CPA are modified for the problem at hand. The frequencies obtained for each example, showing the effect of both beam types, iterations, and boundary conditions. The overall optimisation framework and the computational procedure adopted in this study are illustrated in figure 2.

2.2 *Design variables and constraints*

The design variables considered in this study are the beam width b, thickness h, and material gradation index k. These parameters directly govern the stiffness–mass distribution and dynamic response of FGBs. From a practical perspective, these variables can be effectively controlled during design and manufacturing, making them suitable candidates for optimisation. The beam length L is kept constant throughout the optimisation process to isolate the effects of cross-sectional geometry and material gradation on the natural frequencies. This assumption ensures a fair comparison between optimised configurations and avoids confounding frequency variations caused by changes in span length.

2.3 *Objective function and frequency formulation*

The overall optimisation procedure follows a structured sequence. First, the beam geometry, material properties, and boundary conditions are defined. The natural frequencies are then evaluated using the Euler–Bernoulli beam formulation with spatially varying material properties. Based on these evaluations, the optimisation algorithms iteratively update the design variables b, h and k, while enforcing geometric and material constraints through a penalty-based approach. The process is repeated until the convergence criteria are satisfied, and the optimal design configuration is obtained.

2.4 *Validation of the analytical model*

To verify the accuracy of the analytical formulation adopted in this study, the computed natural frequencies are compared with benchmark closed-form solutions available

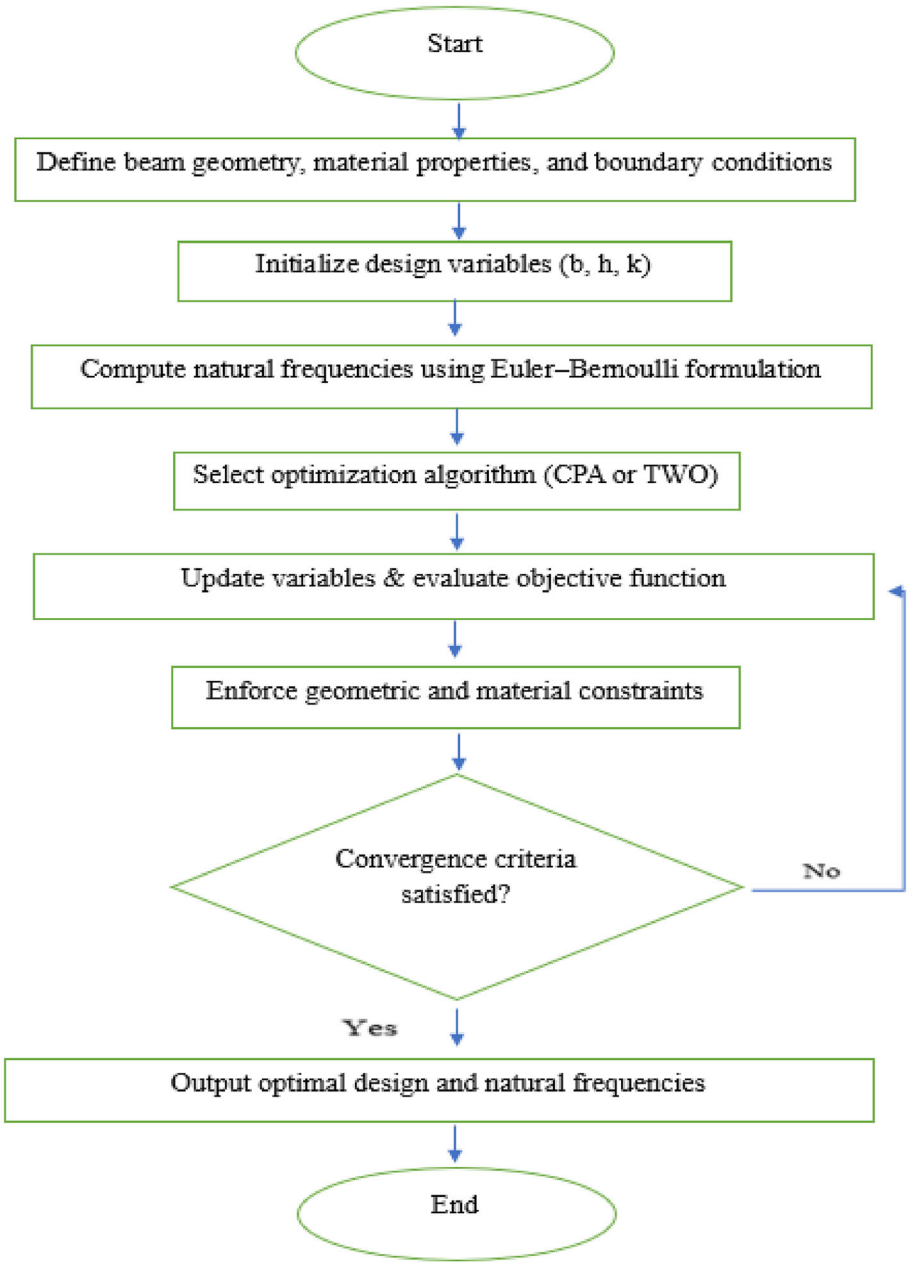


Figure 2. Flowchart of the overall optimisation methodology.

in the literature for functionally graded Euler–Bernoulli beams under classical boundary conditions. In particular, the results are validated against the analytical solutions reported by [49], with a maximum deviation of less than 1.5%, demonstrating excellent agreement. These analytical solutions are widely used as benchmark references for the vibration analysis of FGBs. The comparison shows close agreement between the present results and the benchmark solutions for different boundary conditions and material gradation indices, confirming the correctness and reliability of the adopted formulation. This validation demonstrates that the observed improvements in natural frequencies are attributed to the optimisation process rather than modelling inaccuracies.

2.4.1 *Pseudocode of Cyclical Parthenogenesis algorithm.*

A. Set population size N, maximum iterations $Iter_{\max}$, and bounds of (b, h, k).
B. Generate an initial population of feasible candidate solutions.
C. For each candidate solution,
   i. Evaluate natural frequencies using the Euler–Bernoulli formulation.
   ii. Compute the objective function (maximise the target frequency).
   iii. Apply constraint handling using a penalty function.
D. Identify the current best solution.
E. For $iter = 1$ to $Iter_{\max}$:
   i. Produce new offspring solutions according to the CPA update rule.
   ii. Enforce variable bounds and feasibility constraints.
   iii. Re-evaluate objective and penalty for the new solutions.
   iv. Update the best solution if improvement is achieved.
F. Stop when convergence or $iter_{\max}$ is reached.
G. Return the best design variables and the convergence history

2.4.2 *Pseudocode of Tug of War optimisation algorithm.*

A. Set number of agents N, maximum iterations $iter_{\max}$, and bounds of (b, h, k).
B. Initialise the positions of agents within feasible bounds.
C. For each agent:
   i. Evaluate natural frequencies using the Euler–Bernoulli formulation.
   ii. Compute the objective function and apply penalty-based constraint handling.
D. Rank agents based on fitness values.
E. For $iter = 1$ to $iter_{\max}$:
   i. Compute interaction forces between agents according to TWO rules.
   ii. Update agent positions based on the computed forces.
   iii. Enforce bounds and constraints for updated agents.
   iv. Re-evaluate objective function and update rankings.
F. Stop when convergence or $iter_{\max}$ is reached.
G. Return the best design variables and the convergence history

3. Materials and method

The prismatic beam being examined in this study has a constant length ($L = 500$ mm), width b, and thickness h. The x-axis runs along the beam's longitudinal direction (length), while the y- and z-axis span their cross-sectional width and thickness, respectively. These two right-handed inertial coordinate systems are called x, y, and z. It is ensured that any observed changes in natural frequency are purely due to differences in width, thickness, and material composition rather than beam length by setting L, which isolates the effects of cross-sectional dimensions (b and h) and material grading on dynamic performance. For instance, beams with cross-sectional dimensions of $b = 20$ mm, $h = 30$ mm and $b = 30$ mm, $h = 40$ mm can be directly compared under otherwise identical conditions by keeping the beam length constant at $L = 500$ mm. The beam has length L, width b, and thickness h. Two inertial coordinate systems, denoted by *(x, y, z)*, are considered in the analysis. In this study, the beam length is kept constant at $L = 500$ mm. The material properties used in this study are listed in table 1.

The beam is represented as a functionally graded structure as shown in figure 3, with a metal-rich bottom layer and a ceramic-rich top layer [48].

The beam has a rectangular cross-section (figure 4). The Young's modulus E and density ρ for the typical metal constituents (E_b = 70 GPa, ρ_b = 2700 kg/m^3) and ceramic constituents (E_t = 380 GPa, ρ_t = 3800 kg/m^3) are listed in table 1.

The gradation profile along the thickness is controlled by the volume fraction parameter k (figure 5), which permits the local characteristics to vary constantly between these end-member values in accordance with a power-law distribution. Mass distributions and stiffness may be adjusted due to the graded structure [24].

The material properties of the typical metals and ceramics employed in the study are given in table 1. It is assumed that the top layer of the beam is ceramic-rich and the bottom layer metal-rich. Table 2 presents the constants related to the boundary conditions [49].

3.1 *Design criteria*

The effective cross-section of the area moment about the natural axis is given in eq. (1). It is about its neutral axis computed by integrating the local area moment contributions weighted by the spatially varying Young's modulus [49].

Table 1. Material properties of functionally graded material components.

Material	E (GPa)	p (kg/m^3)
Al	70	2700
Al_2O_3	380	3800

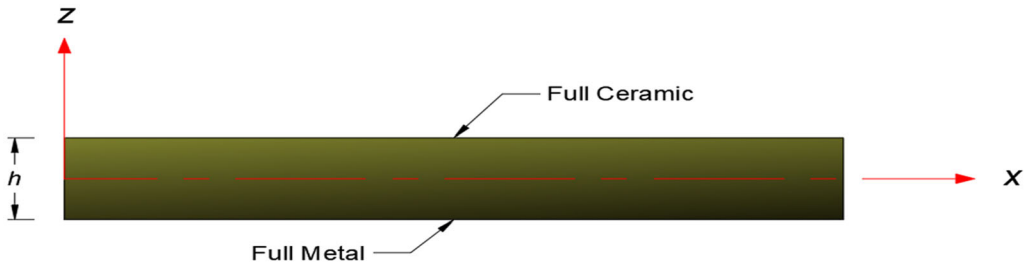


Figure 3. The material properties of functionally graded materials components used.

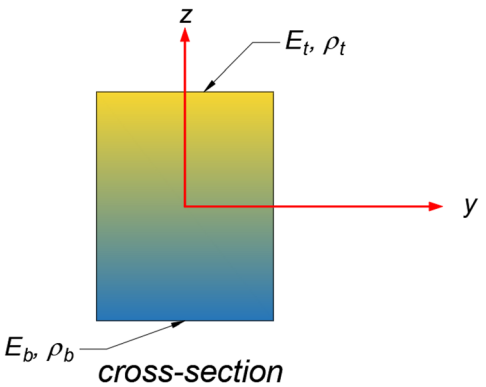


Figure 4. The cross-section of functionally graded materials beam.

$$I_{\text{eff}} = \frac{bh^3}{12}\left[\frac{E_b}{E_t} + 12\left(1 - \frac{E_b}{E_t}\right)\left(\frac{1}{k+3} - \frac{1}{k+2} + \frac{1}{4(k+1)}\right) - \frac{3k^2\left(1 - \frac{E_b}{E_t}\right)^2}{(k+1)(k+2)^2\left(1 + k\frac{E_b}{E_t}\right)}\right] \quad (1)$$

where b is the beam width, h is the beam height, E_b is the modulus of elasticity at the bottom of the beam (bottom-layer Young's modulus, GPa), E_t is the modulus of elasticity at the top of the beam (top-layer Young's modulus, GPa), k is the material gradation parameter. Various volume fraction index k values (numbers at the curves) are shown in figure 4 and the effective mass of the beam is

Table 2. Three values of $\beta_n L$ for beams with various boundary conditions.

Type of beam	$\beta_n L$
Clamped–free	$\beta_1 L$ = 1.875104
	$\beta_2 L$= 4.694091
	$\beta_3 L$= 7.854757
Pinned–pinned	$\beta_1 L$= $\pi\pi$
	$\beta_2 L$= $2\pi 2\pi$
	$\beta_3 L$= $3\pi 3\pi$
Clamped–pinned	$\beta_1 L$= 3.926602
	$\beta_2 L$= 7.068583
	$\beta_3 L$= 10.210176
Clamped–clamped	$\beta_1 L$= 4.730041
	$\beta_2 L$= 7.853205
	$\beta_3 L$= 10.995608

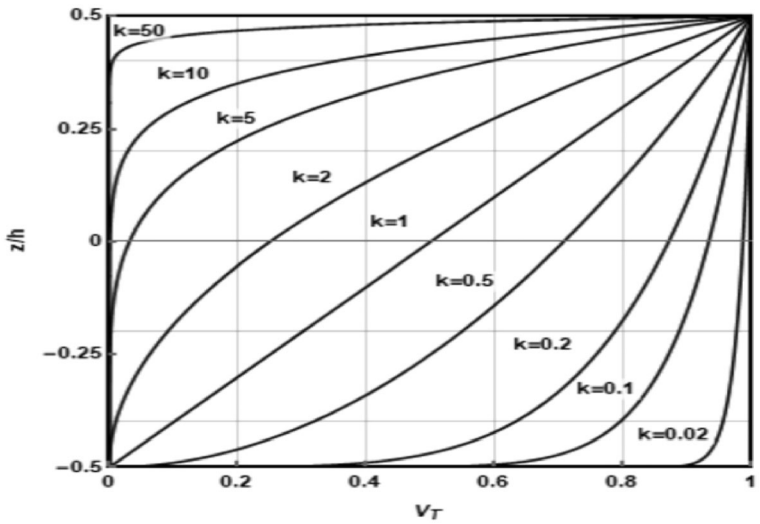


Figure 5. Graphical representation of variation of volume fraction (k).

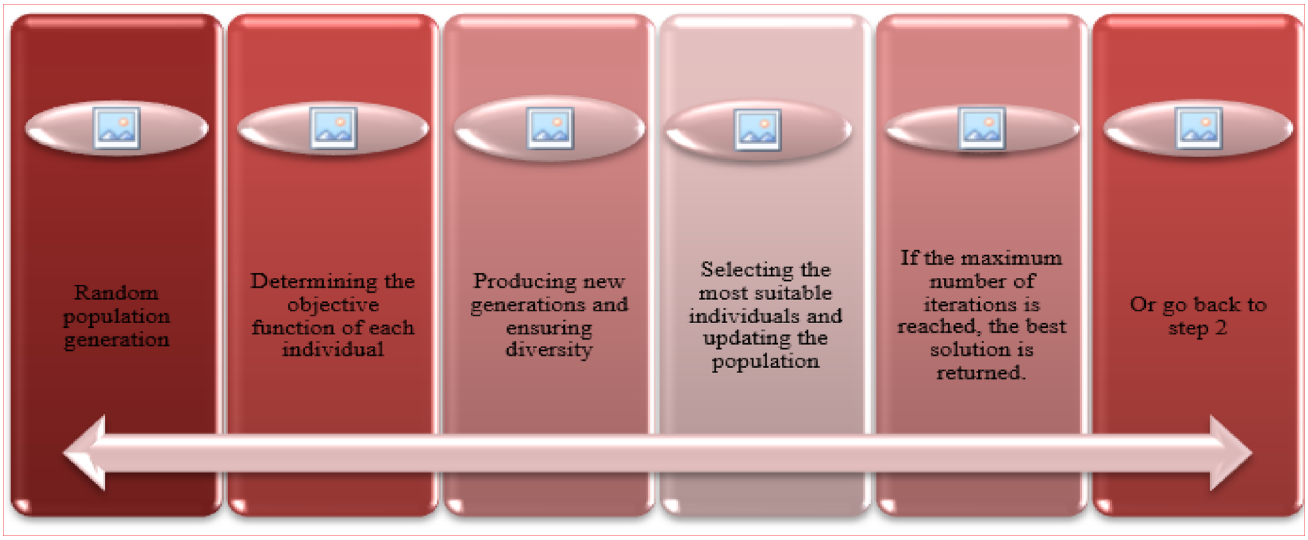


Figure 6. An illustration of the Cyclical Parthenogenesis algorithm flow chart.

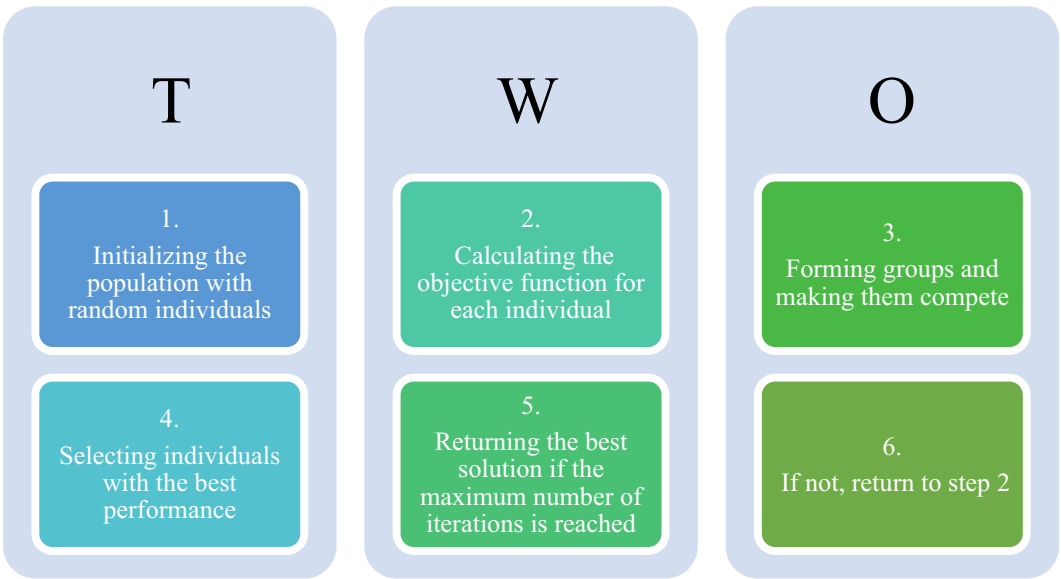


Figure 7. An illustration of Tug of War algorithm flow chart.

presented in eq. (2). It is similarly defined by integrating the local mass per unit length weighted by the square of the mode shape, normalised by the maximum amplitude [49].

$$M_{\text{eff}} = \rho_t bh\left[\frac{\rho_b}{\rho_t} + \left(1 - \frac{\rho_b}{\rho_t}\right)\frac{1}{k+1}\right] \tag{2}$$

where ρ_t is the density at the top of the beam (top-layer density, kg/m^3), ρ_b is the density at the bottom of the beam (bottom-layer density, kg/m^3), k is the material gradation parameter.

3.2 *Objective function*

The natural frequency ω represents the objective function which can be obtained through the classical Euler–Bernoulli relation [49].

$$\omega = (\beta L)^2 \times \frac{(E_t \times I_{\text{eff}})}{(M_{\text{eff}} \times L^4)} \tag{3}$$

where ω is the natural frequency, I_{eff} is the effective moment of area, M_{eff} is the effective mass per unit length, E_t is the effective Young's modulus, and BL is a beam with

Table 3. Cyclical Parthenogenesis algorithm optimised offunctionally graded material clamped–free beam for 10, 20, 30, 40, and 50 iterations (E_b=70, E_t = 380, ρ_t= 3800, ρ_b= 2700).

Optimised of FGM clamped-free beam for 10, 20, 30, 40 and 50 iterations							
Clamped–free NT,s 10	Mode	*BL*	Optimised	Non-dimentional optimisation	*h*	*b*	*k*
	1	$\beta_1 L$ = 1.875104	0.67724	1.145824393	29.02	19.9879	1.56
	2	$\beta_2 L$ = 4.694091	4.2778	6.68242678	31.4306	18.0657	4.1467
	3	$\beta_3 L$ = 7.854757	12.1298	22.20296968	26.8235	17.882	2.433
Clamped–free NT,s 20	1	$\beta_1 L$ = 1.875104	0.67404	1.326340159	24.9519	20.064	3.6088
	2	$\beta_2 L$ = 4.694091	4.2286	8.280560056	25.0732	20.4752	3.7205
	3	$\beta_3 L$ = 7.854757	11.8575	22.41854553	25.9692	20.4083	3.8463
Clamped–free NT,s 30	1	$\beta_1 L$ = 1.875104	0.67192	1.313697281	25.1128	20.0176	4.1331
	2	$\beta_2 L$ = 4.694091	4.2118	8.238822745	25.1001	19.9743	4.363
	3	$\beta_3 L$ = 7.854757	11.7847	23.00500495	25.1518	20.0722	4.4011
Clamped–free NT,s 40	1	$\beta_1 L$ = 1.875104	0.67106	1.316198295	25.033	19.9922	4.4874
	2	$\beta_2 L$ = 4.694091	4.2056	8.265684914	24.9817	19.9941	4.4594
	3	$\beta_3 L$ = 7.854757	11.7765	23.10797455	25.0223	19.9959	4.466
Clamped–free NT,s 50	1	$\beta_1 L$ = 1.875104	0.67081	1.317202321	25.0046	19.9953	4.4804
	2	$\beta_2 L$ = 4.694091	4.2035	8.252770195	25.0083	19.9982	4.4712
	3	$\beta_3 L$ = 7.854757	11.7714	23.10646287	25.0131	19.9943	4.4435

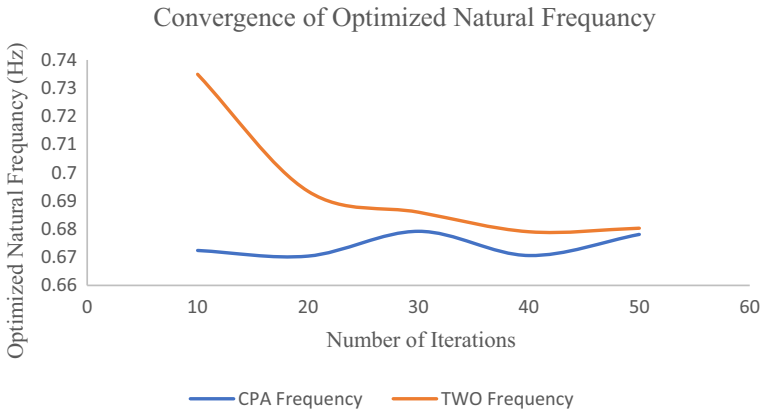


Figure 8. Convergence of optimised natural frequency versus iterations (both algorithms in a clamped–free functionally graded beam).

different boundary conditions. The objective function and design constraints of this research are expressed by special equations represented by the MATLAB program according to the mechanisms of the CPA and TWO algorithms. The boundary in this case is assumed to be as

$$10 < b < 40, 20 < h < 50, \text{ and } 1 < k < 10.$$

The maximum number of objective function evaluations can be expressed as 20,000.

The non-dimensional frequency λ and the variation in the volume fraction V_t can be obtained by equations (4) and (5) respectively.

$$\lambda = \left(\frac{\omega L^2}{h}\right)\sqrt{\frac{\rho_b}{E_b}} \tag{4}$$

$$V_t = \left(\frac{(2z+h)}{2h}\right)^{\kappa} \tag{5}$$

The effective Young's modulus $E(z)$ and the mass density $\rho(z)$ are expressed as

$$E(z) = E_b + (E_t - E_b) \times \left(\frac{(2z+h)}{2h}\right)^{\kappa} \tag{6}$$

$$\rho(z) = \rho_b + (\rho_t - \rho_b) \times \left(\frac{(2z+h)}{2h}\right)^{\kappa} \tag{7}$$

3.3 *Cyclical Parthenogenesis algorithm*

The Cyclical Parthenogenesis algorithm is the first algorithm used in this study, and the flowchart of the CPA

Table 4. Cyclical Parthenogenesis algorithm optimised functionally graded material pinned–pinned beam for 10, 20, 30, 40, and 50 iterations for the same material (table 1).

Optimised of functionally graded material clamped–pinned beam for 10, 20, 30, 40 and 50 iterations							
	Mode	*BL*	Optimised	Non-dimentional optimisation	*h*	*b*	*k*
Clamped–pinned NIT,s 10	1	$\beta_1 L = 3.926602$	3.0183	5.090095591	29.1145	19.4333	2.5494
	2	$\beta_2 L = 7.068583$	9.8948	16.70357109	29.0851	18.4405	4.5276
	3	$\beta_3 L = 10.210176$	20.2701	33.62111476	29.6017	18.2533	4.7456
Clamped–pinned NIT,s 20	1	$\beta_1 L = 3.926602$	2.9588	5.703871943	25.4694	20.1363	3.899
	2	$\beta_2 L = 7.068583$	9.6008	18.58888358	25.3587	20.0687	3.7762
	3	$\beta_3 L = 10.210176$	20.0425	38.88348847	25.3081	19.9185	3.4431
Clamped–pinned NIT,s 30	1	$\beta_1 L = 3.926602$	2.9466	5.74588993	25.1789	19.9573	4.3083
	2	$\beta_2 L = 7.068583$	9.5426	18.64530831	25.1287	19.9458	3.8046
	3	$\beta_3 L = 10.210176$	19.941	39.07176233	25.0586	20.098	4.2112
Clamped–pinned NIT,s 40	1	$\beta_1 L = 3.926602$	2.9427	5.76965505	25.042	19.9684	4.4968
	2	$\beta_2 L = 7.068583$	9.5363	18.72045975	25.0113	19.9923	4.3711
	3	$\beta_3 L = 10.210176$	19.9045	39.02812418	25.0407	20.0222	4.5061
Clamped–pinned NIT,s 50	1	$\beta_1 L = 3.926602$	2.9415	5.776760247	25.001	20.0018	4.4839
	2	$\beta_2 L = 7.068583$	9.5321	18.71393575	25.009	19.9916	4.5207
	3	$\beta_3 L = 10.210176$	19.8888	39.04880075	25.0077	19.9953	4.4985

Table 5. Cyclical Parthenogenesis algorithm optimised functionally graded material clamped–pinned beam for 10, 20, 30, 40, and 50 iterations for the same material (table 1).

Optimised of functionally graded material clamped–pinned beam for 10, 20, 30, 40 and 50 iterations							
	Mode	*BL*	Optimised	Non-dimentional optimisation	*h*	*b*	*k*
Clamped–pinned NIT,s 10	1	$\beta_1 L = 3.926602$	3.0183	5.090095591	29.1145	19.4333	2.5494
	2	$\beta_2 L = 7.068583$	9.8948	16.70357109	29.0851	18.4405	4.5276
	3	$\beta_3 L = 10.210176$	20.2701	33.62111476	29.6017	18.2533	4.7456
Clamped–pinned NIT,s 20	1	$\beta_1 L = 3.926602$	2.9588	5.703871943	25.4694	20.1363	3.899
	2	$\beta_2 L = 7.068583$	9.6008	18.58888358	25.3587	20.0687	3.7762
	3	$\beta_3 L = 10.210176$	20.0425	38.88348847	25.3081	19.9185	3.4431
Clamped–pinned NIT,s 30	1	$\beta_1 L = 3.926602$	2.9466	5.74588993	25.1789	19.9573	4.3083
	2	$\beta_2 L = 7.068583$	9.5426	18.64530831	25.1287	19.9458	3.8046
	3	$\beta_3 L = 10.210176$	19.941	39.07176233	25.0586	20.098	4.2112
Clamped–pinned NIT,s 40	1	$\beta_1 L = 3.926602$	2.9427	5.76965505	25.042	19.9684	4.4968
	2	$\beta_2 L = 7.068583$	9.5363	18.72045975	25.0113	19.9923	4.3711
	3	$\beta_3 L = 10.210176$	19.9045	39.02812418	25.0407	20.0222	4.5061
Clamped–pinned NIT,s 50	1	$\beta_1 L = 3.926602$	2.9415	5.776760247	25.001	20.0018	4.4839
	2	$\beta_2 L = 7.068583$	9.5321	18.71393575	25.009	19.9916	4.5207
	3	$\beta_3 L = 10.210176$	19.8888	39.04880075	25.0077	19.9953	4.4985

procedure is presented in figure 6. This algorithm is a design and optimisation method that uses standard parameters and classical formulas from dynamics and solid mechanics. It depends on established design rules, engineering intuition, and analytical formula's. In this case, the natural frequency is optimised using standard cross-sectional properties.

3.4 *Tug of war algorithm*

The TWO algorithm is the second used algorithm. Figure 7 illustrates the flowchart of the proposed optimisation algorithm. It simplifies the optimisation process by limiting the number of variables. It has several effects on design, such as computational efficiency, better balance between performance and manufacturability, insight into dominant design parameters, and facilitates parametric studies. In this case, it enhances and optimises beam dimensions for stiffness, frequency, or strength, especially Tailor component geometry to avoid resonance. The theory, assumptions, restrictions, and formulation about these two algorithms can be found in [50]. This study focuses on the application of these algorithms to the free vibration optimisation of FGBs rather than the theory of optimisation.

Table 6. Cyclical Parthenogenesis algorithm optimised functionally graded material clamped–clamped beam for 10, 20, 30, 40, and 50 iterations for the same material (table 1).

Optimised of funtionally graded material clamped–clamped beam for 10, 20, 30, 40 and 50 iterations							
Clamped–clamped NIT,s 10	Mode	*BL*	Optimised	Non-dimentional optimisation	*h*	*b*	*k*
	1	$\beta_1 L = 4.730041$	4.3143	7.312126757	28.9694	18.0869	4.469
	2	$\beta_2 L = 7.853205$	12.0611	22.59156802	26.2128	20.3577	1.8086
	3	$\beta_3 L = 10.995608$	23.3181	39.350942	29.0945	21.9612	2.4084
Clamped–clamped NIT,s 20	1	$\beta_1 L = 4.730041$	4.2939	8.391764708	25.123	19.917	3.9871
	2	$\beta_2 L = 7.853205$	11.8657	22.92865932	25.409	20.0041	3.0835
	3	$\beta_3 L = 10.995608$	23.2016	44.65605431	25.51	19.7567	3.6583
Clamped–clamped NIT,s 30	1	$\beta_1 L = 4.730041$	4.2764	8.369256566	25.0879	20.041	4.3728
	2	$\beta_2 L = 7.853205$	11.7786	23.11532845	25.0188	20.0286	4.1711
	3	$\beta_3 L = 10.995608$	23.1114	45.44988238	24.967	20.0209	4.2422
Clamped–clamped NIT,s 40	1	$\beta_1 L = 4.730041$	4.2691	8.373761522	25.0316	20.001	4.4174
	2	$\beta_2 L = 7.853205$	11.7656	23.06787203	25.0426	19.9944	4.5447
	3	$\beta_3 L = 10.995608$	23.0745	45.2401482	25.0427	19.9742	4.4431
Clamped-clamped NIT,s 50	1	$\beta_1 L = 4.730041$	4.2683	8.38026071	25.0075	20.0014	4.4657
	2	$\beta_2 L = 7.853205$	11.7662	23.10262861	25.0062	20.0019	4.4639
	3	$\beta_3 L = 10.995608$	23.0654	45.30878932	24.9949	19.9982	4.4818

Table 7. The results of the TWO optimised functionally graded material clamped–free beam for 10, 20, 30, 40, and 50 iterations by the same materials (table 1).

	Mode	*BL*	Optimised	Non-dimentional optimisation	*b*	*h*	*k*
Clamped–free NT,s 10	1	$\beta_1 L = 1.875104$	0.73492	1.521126376	25.1608	23.7218	5.3139
	2	$\beta_2 L = 4.694091$	4.3319	9.288796155	26.6568	22.8977	3.5468
	3	$\beta_3 L = 7.854757$	12.4644	27.75288149	23.794	22.0514	3.4042
Clamped–free NT,s 20	1	$\beta_1 L = 1.875104$	0.69341	1.107474355	16.8538	30.7418	9.525
	2	$\beta_2 L = 4.694091$	4.3352	7.617302575	18.0154	27.9435	8.8027
	3	$\beta_3 L = 7.854757$	12.3419	18.17398736	15.4383	33.343	8.7069
Clamped–free NT,s 30	1	$\beta_1 L = 1.875104$	0.68598	0.847129809	13.626	39.7589	4.5044
	2	$\beta_2 L = 4.694091$	4.2929	7.917406871	21.3773	26.622	3.9722
	3	$\beta_3 L = 7.854757$	11.9174	13.92708916	15.8218	42.014	4.5388
Clamped–free NT,s 40	1	$\beta_1 L = 1.875104$	0.67904	1.024918909	15.443	32.5296	1.6917
	2	$\beta_2 L = 4.694091$	4.264	7.420472534	21.4941	28.2136	1
	3	$\beta_3 L = 7.854757$	11.9209	17.17831114	19.9479	34.0723	3.4704
Clamped–free NT,s 50	1	$\beta_1 L = 1.875104$	0.6803	1.239339811	20.8233	26.9515	1
	2	$\beta_2 L = 4.694091$	4.2376	7.742851334	19.8898	26.8715	1
	3	$\beta_3 L = 7.854757$	11.9469	22.06112872	19.5481	26.5889	1

4. Results and discussion

This chapter examines the results obtained by MATLAB using both methods, CPA and TWO. It shows the optimum frequencies related to the materials and constraints. Using both methods with different types of beams can differ in frequency. The constraints and boundaries are presented in Section 3.

4.1 *Results obtained by Cyclical Parthenogenesis algorithm*

First, a convergence study is conducted to determine the appropriate number of iterations. For this purpose, CPA is implemented to optimise FGBs with clamped–free (C–F) boundary conditions. The results obtained for different numbers of iterations are presented in table 3.

In the clamped–free condition (table 3), the CPA algorithm shows a noticeable convergence after 20 iterations, as the natural frequencies change between 10 and 20 iterations and become almost stable after the 30^{th} iteration. In addition, there is an early stability in the geometric dimensions of the cross-section, namely the width and height, as they change very slightly, less than half a millimeter. Figure 8 illustrates the convergence histories of the optimised fundamental natural frequency (Mode 1) with respect to the number of iterations for both CPA and TWO under clamped–free boundary conditions free boundary conditions. Both algorithms exhibit smooth and

Table 8. The results of the TWO optimised functionally graded material pinned–pinned beam for 10, 20, 30, 40, and 50 iterations by the same materials (table 1).

	Mode	*BL*	Optimised	Non-dimentional optimisation	*b*	*h*	*k*
Pinned–pinned NT,s 10	1	$\beta_1 L = p$	1.9428	4.579718675	24.5683	20.8287	6.7528
	2	$\beta_2 L = 2\ p$	8.0904	16.28001567	27.3145	24.3999	3.241
	3	$\beta_3 L = 3\ p$	17.7809	36.86231111	25.0083	23.6834	8.8241
Pinned–pinned NT,s 20	1	$\beta_1 L = p$	1.9635	2.405986049	17.179	40.0692	7.6023
	2	$\beta_2 L = 2\ p$	7.8877	11.05874575	16.4176	35.0201	8.2108
	3	$\beta_3 L = 3\ p$	17.7958	22.66853551	13.5609	38.5449	10
Pinned–pinned NT,s 30	1	$\beta_1 L = p$	1.9079	3.51768796	19.9116	26.63	4.5571
	2	$\beta_2 L = 2\ p$	7.6703	14.12152979	19.0299	26.6688	4.555
	3	$\beta_3 L = 3\ p$	17.2946	20.13678302	16.2492	42.169	1
Pinned–pinned NT,s 40	1	$\beta_1 L = p$	1.9009	2.909207966	20.0233	32.0817	2.3676
	2	$\beta_2 L = 2\ p$	7.5861	12.61357756	23.5493	29.5293	1
	3	$\beta_3 L = 3\ p$	17.1039	22.97720895	15.8817	36.5486	3.9288
Pinned–pinned NT,s 50	1	$\beta_1 L = p$	1.8867	2.842300809	19.6223	32.5916	4.3716
	2	$\beta_2 L = 2\ p$	7.5821	13.76701009	19.3369	27.041	1
	3	$\beta_3 L = 3\ p$	17.1274	30.75877095	20.1262	27.3398	1

Table 9. The results of the TWO optimised of the functionally graded material clamped–pinned beam for 10, 20, 30, 40, and 50 iterations by the same materials (table 1).

	Mode	*BL*	Optimised	Non-dimentional optimisation	*b*	*h*	*k*
Clamped–pinned NIT,s 10	1	$\beta_1 L = 3.926602$	3.177	6.120905471	25.691	25.4844	1
	2	$\beta_2 L = 7.068583$	9.7655	19.55211563	28.4443	24.523	1.5515
	3	$\beta_3 L = 10.210176$	20.7396	42.05550488	28.5027	24.2131	1
Clamped–pinned NIT,s 20	1	$\beta_1 L = 3.926602$	2.949	4.827109983	17.8771	29.9958	9.3006
	2	$\beta_2 L = 7.068583$	9.8371	16.43305111	17.7966	29.3915	9.5845
	3	$\beta_3 L = 10.210176$	20.3271	29.32817703	14.7485	34.0301	10
Clamped–pinned NIT,s 30	1	$\beta_1 L = 3.926602$	3.0232	4.21880644	16.258	35.1844	1
	2	$\beta_2 L = 7.068583$	9.6102	17.58716973	19.5643	26.8293	4.7177
	3	$\beta_3 L = 10.210176$	20.2064	35.285346	19.6154	28.1169	4.6663
Clamped–pinned NIT,s 40	1	$\beta_1 L = 3.926602$	2.9929	5.184995389	19.5405	28.3411	1
	2	$\beta_2 L = 7.068583$	9.5873	14.09404+E15:E2272854994	17.7285	33.399	3.4875
	3	$\beta_3 L = 10.210176$	20.1281	31.97395195	20.0324	30.9086	1
Clamped–pinned NIT,s 50	1	$\beta_1 L = 3.926602$	2.9616	4.620967253	19.5154	31.4678	4.0392
	2	$\beta_2 L = 7.068583$	9.6408	16.66639262	18.1415	28.4017	1.6688
	3	$\beta_3 L = 10.210176$	19.9623	35.28450577	20.5123	27.7779	1

stable convergence trends without abrupt oscillations, confirming the numerical reliability of the optimisation process. CPA demonstrates relatively rapid stabilisation at early iterations, whereas TWO shows a more gradual convergence behaviour, consistent with its broader exploration strategy. These observations support the reliability of the tabulated optimisation results reported in tables 3 and 7.

For the pinned–pinned boundary condition (table 4), the CPA exhibits a substantial reduction between 10 and 20 iterations, particularly in the second vibration mode, with a maximum decrease of approximately 13%, however, at iteration 30, all frequencies stabilise from their final values by a value of up to 1%. The design dimensions show only minor changes after iteration 30, indicating very effective convergence.

In the clamped–pinned condition (table 5), the CPA algorithm shows large changes in dimensions of up to about 15% at iterations between 10 and 20, especially in the first mode, but the frequency changes gradually and decrease by the 40th iteration to reach 0.3%, with the dimensions (*b* and *h*) stabilising within 9% of their final value. This indicates that the CPA algorithm has the ability to achieve stability when dynamic developments.

In the clamped–clamped condition (table 6), the CPA algorithm shows the fastest convergence in all cases, as after 30 iterations, the frequency changes decrease to $<$ 0.05, and the width *b* to $<$ 0.05 mm, while the design variables after 40 iterations become almost constant. This indicates the effective and strong effect of the boundary constraints in accelerating the optimisation process.

Table 10. The results of the TWO optimised functionally graded material clamped–clamped beam for 10, 20, 30, 40, and 50 iterations by the same materials (table 1)

	Mode	*BL*	Optimised	Non-dimentional optimisation	*b*	*h*	*k*
Clamped–clamped NIT,s 10	1	$\beta_1 L = 4.730041$	4.6944	9.125552381	25.9563	25.2577	3.1084
	2	$\beta_2 L = 7.853205$	12.6695	27.1039524	24.6184	22.9509	3.2798
	3	$\beta_3 L = 10.995608$	24.5092	48.63370599	26.9209	24.7437	8.6761
Clamped–clamped NIT,s 20	1	$\beta_1 L = 4.730041$	4.3545	8.012355932	20.2432	26.684	8.6095
	2	$\beta_2 L = 7.853205$	12.1565	19.78921145	21.615	30.1615	7.1249
	3	$\beta_3 L = 10.995608$	23.9902	35.00692286	16.3743	33.6475	8.34
Clamped–clamped NIT,s 30	1	$\beta_1 L = 4.730041$	4.3624	8.040089338	19.9768	26.6402	4.762
	2	$\beta_2 L = 7.853205$	12.2104	14.89909536	16.1116	40.2386	4.4596
	3	$\beta_3 L = 10.995608$	23.2826	42.27230246	20.6728	27.0426	4.9078
Clamped–clamped NIT,s 40	1	$\beta_1 L = 4.730041$	4.3104	6.309783211	19.9813	33.541	1.7477
	2	$\beta_2 L = 7.853205$	11.9342	19.88507859	19.3031	29.4672	1
	3	$\beta_3 L = 10.995608$	23.392	35.21536258	19.6863	32.6143	1.7102
Clamped–clamped NIT,s 50	1	$\beta_1 L = 4.730041$	4.2901	7.625602438	18.4732	27.6227	1
	2	$\beta_2 L = 7.853205$	11.8358	18.66466604	21.0518	31.1351	3.4985
	3	$\beta_3 L = 10.995608$	23.3394	37.90166866	22.4806	30.2346	2.9241

As a result, the CPA algorithm shows good early convergence across all four cases, with major improvements occurring within the first 20 iterations, especially in the first mode. Most designs stabilise at iteration 30 with only a few geometric changes. The beams clamped–clamped show faster convergence due to the boundary constraints. Thus, this algorithm demonstrates effective performance in achieving reliable optimisation at low iterations for all cases in this study.

In this part, the convergence study for TWO will be carried out. The obtained results for C–F are presented in table 7.

In the clamped–free condition (table 7, the TWO algorithm shows a gradual improvement and stability in the frequencies during the first 20 iterations, as both the height *h* and width *b* have average changes between patterns. This indicates that there is a stable convergence, but it is relatively slow, as the algorithm requires a long processing time.

In the pinned–pinned condition (table 8), the TWO algorithm shows irregular convergence between the modes, where fluctuations are observed, especially at the third mode. In addition, there is an improvement in the frequency values with repetition, but the geometric dimensions vary greatly, which indicates a relatively limited stability and a higher sensitivity to this type of beams.

The material gradient index *k* is a high value at the beginning, which requires large cross-sections to maintain rigidity, noting that it decreases at the 50^{th} repetition to reach a value of one, which in turn indicates a transition towards better control of frequencies and towards a denser material.

In the clamped–pinned condition (table 9), the performance of the TWO algorithm is moderately stable, as the gradient values improve gradually, but the geometric dimensions of the watch undergo moderate changes across iterations. As for the material gradient index *k*, it has a high value, especially in the first mode, then it decreases again to reach a value of one at iteration 50. This indicates a transition towards the use of denser materials with better control at higher iterations in terms of stiffness.

In the clamped–clamped condition (table 10), especially in the first and second modes, the TWO algorithm shows a relatively smooth convergence in frequencies. As for the third mode, there is a large variation in the geometric dimensions and the material gradation index *k*, as it starts with high values and drops to less than three at iteration 50. This reflects the mechanism of transitioning towards more rigid and stable materials in geometric dimensions at iteration 40, which in turn is a late structural convergence compared to the other cases.

Considering the overall set of tabulated results obtained for both optimisation algorithms, the enhancement of natural frequencies is governed by the combined influence of cross-sectional geometry, material gradation, and boundary conditions. Variations in beam thickness primarily affect stiffness dominance, whereas changes in width influence mass distribution. The material gradation index further modifies this balance by redistributing stiffness across the thickness, which explains the non-linear trends observed in the optimised designs. These interactions highlight the importance of simultaneous geometric and material optimisation rather than treating each parameter independently. A comparative interpretation of the results indicates that the CPA algorithm tends to converge toward conservative design configurations characterised by moderate gradation indices and stable geometric dimensions. This behaviour reflects its emphasis on feasibility and early convergence. In contrast, the TWO algorithm explores a broader design space, allowing more pronounced variations in geometry

Table 11. Material properties of functionally graded material components.

Functionally graded material beam type	E_b(GPa)	ρ_b(kg/m^3)	E_t(GPa)	ρ_t(kg/m^3)
Clamped–free	70	2700	140	3800
Pinned–pinned	70	2700	280	3800
Clamped–pinned	70	2700	500	3800
Clamped–clamped	70	2700	380	5400

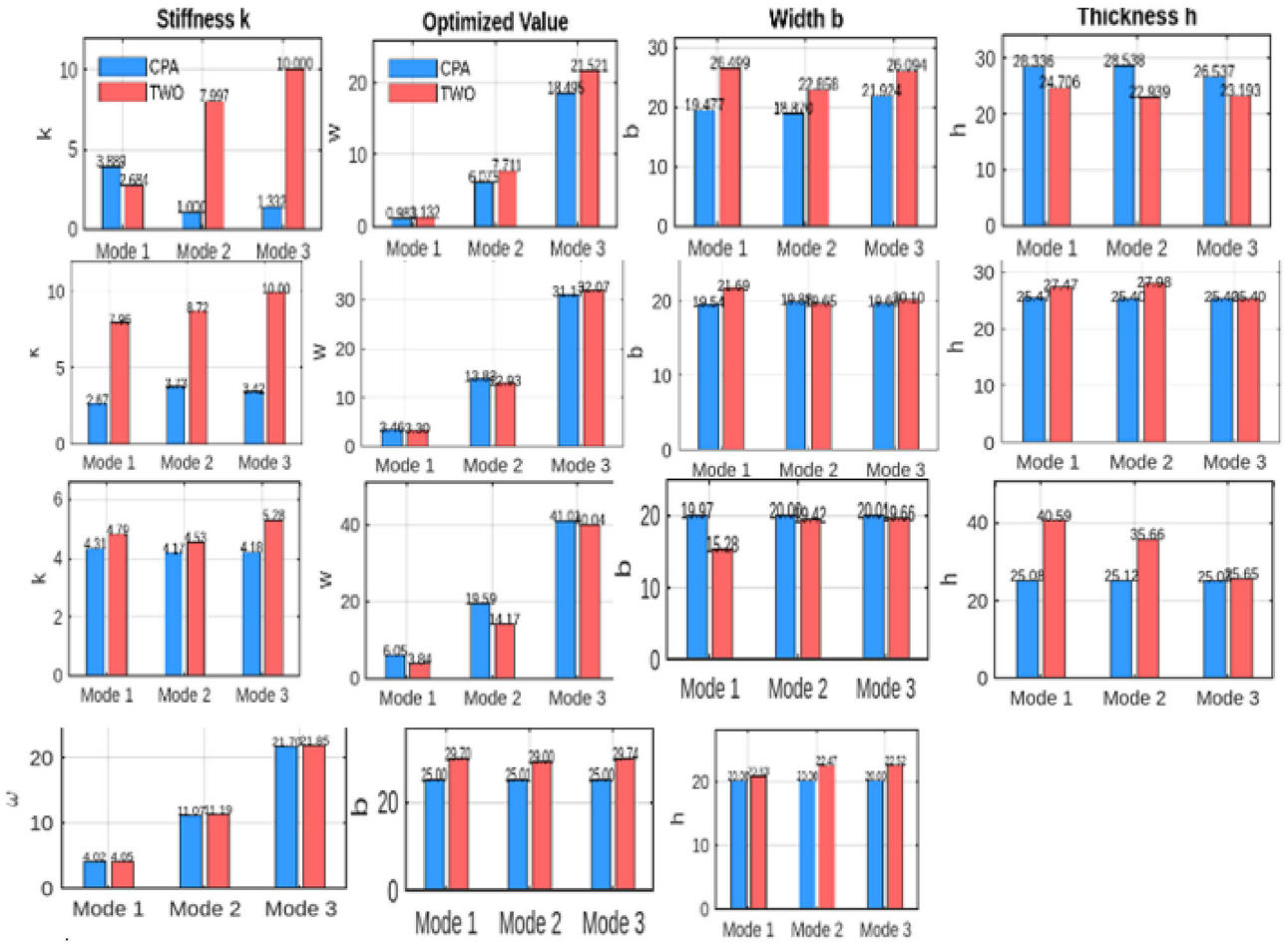


Figure 9. Comparison of Tug of War optimisation and Cyclical Parthenogenesis algorithms for functionally graded material beams: Gradient Index, frequency, width, and height.

and material distribution, which leads to higher achievable natural frequencies in several cases. The observed differences are consistent with the distinct search mechanisms of the two algorithms and explain the performance gaps reported in the tabulated results. The influence of boundary conditions is clearly reflected in the optimisation outcomes. Beams with clamped–clamped constraints exhibit higher natural frequencies and faster convergence due to increased rotational restraint, whereas clamped–free configurations show greater sensitivity to geometric variations. These trends are in agreement with classical vibration theory and further support the physical validity of the obtained results.

Furthermore, the optimised natural frequencies exhibit consistent and smooth variations across different beam configurations, boundary conditions, and iteration levels, indicating stable convergence of the optimisation process. The absence of abrupt fluctuations or contradictory trends in the tabulated results confirms that the reported solutions are numerically stable and represent converged optimal designs rather than incidental outcomes of the search process.

4.2 *Comparison of the performance of Tug of War optimisation and Cyclical Parthenogenesis algorithms in functionally graded material beam design*

This section aims to evaluate the effectiveness of two algorithms, TWO and CPA, in improving the response of FGM beams under different constraining conditions by conducting a comprehensive comparison between these two algorithms based on a set of design and performance indicators for the four types of FGM beams.

4.2.1 *Comparison by functionally graded material beam type.* The results in tables from 3–10 show that the performance of the two algorithms differs depending on the type of constraint on the FGM beam. In the clamped–free beam, the CPA algorithm outperforms the TWO by producing frequencies with thin dimensions and a low gradient coefficient, which indicates a reduction in cost and an increase in stiffness. As for the pinned–pinned beam, the TWO outperforms in the third mode through its design for wider sections and a larger gradient coefficient. As for the clamped–pinned beam, the two algorithms show a largely similar performance, with improved performance, but the CPA algorithm shows better performance because it is characterised by a variable physical gradient and more precise control of dimensions. In the fourth type of beams clamped–clamped beam, the CPA algorithm maintains its design flexibility, while the TWO relies on a fixed gradient coefficient and larger dimensions.

4.2.2 *Comparison by using different material: Properties*. Comparing CPA and TWO across different material properties helps validate the robustness of each optimisation method and understand the sensitivity of the optimisation outcomes to changes in material properties. New material properties are given in table 11.

According to figure 9, which represents a comprehensive comparison between the CPA and TWO algorithms for the four FGM beams used in this study, each beam differs in terms of the type of constraint and material properties, as shown in table 11. This figure shows that the CPA algorithm shows a high k of 10 and a high frequency in the clamped–free beam, while the TWO algorithm has more balanced dimensions and a lower gradient factor. As for the pinned–pinned beam, the CPA algorithm maintained relatively average values, while the TWO algorithm gives slightly better performance in terms of width and frequency by raising the k to about 7. In the clamped–pinned beam, the CPA algorithm shows stable results as it has integrated dimensions, while the TWO algorithm increases k and dimensions significantly to increase the frequency. For the fourth clamped–clamped beam, the CPA algorithm maintains a traditional design with fixed dimensions, whereas the TWO algorithm modifies the coefficient. The gradation pattern results in a higher frequency as the beam height increases, which is generally observed.

At last, the CPA algorithm is characterised by more conservative designs and is easier to manufacture, while the TWO algorithm shows greater flexibility in controlling the dimensions of the beam and the distribution of the material, especially when there is a need for high density or high stiffness.

5. Conclusion

In this study, a comparison is made between two new generation algorithms, CPA and TWO. The results reached and expressed in the tables and figures in this study strongly support the following conclusions: The aim is to improve the natural frequencies of two-layer FGM beams using four constraint cases. This includes a detailed analysis of the effect of the main geometric dimensions, namely length, height, and width, in addition to the material gradient factor, on the dynamic performance of these beams. In addition, the performance of each of the two algorithms is evaluated and compared under multiple vibrations and through the effect of changes in the mechanical properties of the materials used. This aims to verify the effectiveness, efficiency, and robustness of each algorithm under different design conditions. The results are as follows:

Quantitative evaluation of the optimised results shows that both CPA and TWO enhance the natural frequencies of FGBs under classical boundary conditions, with TWO achieving higher improvements of up to 25% in several cases. While CPA exhibits faster and more stable convergence suitable for conservative designs, TWO is more effective when maximum vibration performance is the primary objective. CPA and TWO are used to minimise the natural frequencies of FGM beams under four classical boundary conditions. CPA produced height-dominated conservative designs with moderate gradient index values. In contrast, TWO exploited a wider design space, optimising multi-mode frequency gains through adaptive geometry and material distribution. Design priorities are the most important factor in determining the most appropriate choice between the two algorithms. In cases of lightweight, manufacturable solutions with moderate performance goals, it is preferable to use the CPA algorithm. However, in high-frequency designs that focus on robustness in advanced applications such as space and devices, here the TWO algorithms must be chosen. The layered manufacturing techniques used to extend the optimisation to 3D shell-like FG structures, in addition to the adaptive flexibility of the TWO algorithm and the deterministic region hybridisation of the CPA algorithm, should be considered in future research.

References

[1] Noori A R, Aslan T A and Temel B 2020 Static analysis of FG beams via complementary functions method. *Eur. Mech. Sci.* 4: 1–6.

[2] Birman V and Byrd L W 2007 Modeling and analysis of functionally graded materials and structures. *Appl. Mech. Rev.* 60: 195–216.

[3] Aydogdu M and Taskin V 2007 Free vibration analysis of functionally graded beams with simply supported edges. *Mater. Des.* 28: 1651–1656.

[4] Sina S A, Navazi H M and Haddadpour H 2009 An analytical method for free vibration analysis of functionally graded beams. *Mater. Des.* 30: 741–747.

[5] Simsek M 2010 Vibration analysis of a functionally graded beam under a moving mass by using different beam theories. *Compos. Struct.* 92: 904–917.

[6] Masjedi P K, Maheri A and Weaver P M 2019 Large deflection of functionally graded porous beams based on a geometrically exact theory with a fully intrinsic formulation. *Appl. Math. Model.* 76: 938–957.

[7] Noori A R, Aslan T A and Temel B 2021 Dynamic analysis of functionally graded porous beams using complementary functions method in the Laplace domain. *Compos. Struct.* 256: 113094.

[8] Rasooli H, Noori A R and Temel B 2024 Static analysis of functionally graded porous beam-column frames by the complementary functions method. *Structures* 62: 106136.

[9] Benadouda M, El Amin B M, Dahmane M, Bennai R, Ait Atmane H and Safer O 2025 Dynamic response of wave propagation in functionally graded beams with defects: effects of porosity and cracks. *Acta Mech.* 236: 2279–2296.

[10] Joshi K K, Kar V R and Kumar S 2025 Nonlinear bending characteristics of multidirectional functionally graded porous panels using higher-order finite element solution with parametric optimisation. *Mech. Adv. Mater. Struct.* 32: 169–193.

[11] Thai H T and Vo T P 2012 Bending and free vibration of functionally graded beams using various higher-order shear deformation beam theories. *Int. J. Mech. Sci.* 62: 57–66.

[12] Wattanasakulpong N and Ungbhakorn V 2012 Free vibration analysis of functionally graded beams with general elastically end constraints by DTM. *World J. Mech.* 2: 297–310.

[13] Tsiatas G C and Charalampakis A E 2017 Optimising the natural frequencies of axially functionally graded beams and arches. *Compos. Struct.* 160: 256–266.

[14] Amir M and Kim S W 2024 A study of the natural frequencies of the functionally graded curved beams including porosities: deterministic and stochastic modeling. *Mech. Based Des. Struct. Mach.* 52: 5970–5987.

[15] Al-Zahrani M A, Asiri S A, Ahmed K I and Eltaher M A 2022 Free vibration analysis of 2D functionally graded strip beam using finite element method. *J. Appl. Comput. Mech.* 8: 1422–1430.

[16] Alshorbagy A E, Eltaher M A and Mahmoud F 2011 Free vibration characteristics of a functionally graded beam by finite element method. *Appl. Math. Model.* 35: 412–425.

[17] Nikbakht S, Kamarian S and Shakeri M 2019 A review on optimisation of composite structures Part II: Functionally graded materials. *Compos. Struct.* 214: 83–102.

[18] Anandrao K S, Gupta R K, Ramachandran P and Rao G V 2012 Free vibration analysis of functionally graded beams. *Def. Sci. J.* 62: 139–146.

[19] Keleshteri M M and Jelovica J 2022 Analytical assessment of nonlinear forced vibration of functionally graded porous higher order hinged beams. *Compos. Struct.* 298: 115994.

[20] Pradhan K K and Chakraverty S 2013 Free vibration of Euler and Timoshenko functionally graded beams by Rayleigh-Ritz method. *Compos. Part B Eng.* 51: 175–184.

[21] Huang Y and Li X F 2010 Bending and vibration of circular cylindrical beams with arbitrary radial nonhomogeneity. *Int. J. Mech. Sci.* 52: 595–601.

[22] Murin J, Aminbaghai M, Hrabovsky J, Kutis V, Paulech J and Kugler S 2014 A new 3D FGM beam finite element for modal analysis. In: Proceedings of the 11th World Congress on Computational Mechanics (WCCM 2014), 5th European Conference on Computational Mechanics (ECCM 2014) and 6th European Conference on Computational Fluid Dynamics (ECFD 2014), Barcelona, Spain. pp. 2810–2821.

[23] Li X F, Kang Y A and Wu J X 2013 Exact frequency equations of free vibration of exponentially functionally graded beams. *Appl. Acoust.* 74: 413–420.

[24] Ozmen U and Ozhan B B 2025 Mechanics of functionally graded beams: analytical, computational, and experimental analyses. *Int. J. Mech. Mater. Des.* 21: 577–590.

[25] Albayati M A S and Noori A R 2024 Uc Farkli Metasezgesel Algoritma Kullanilarak Petek Kirislerin Yer Degistirme Optimisasyonu. *Cukurova Univ. Muh. Fak. Derg.* 39: 979–990.

[26] Albayati M A S, Noori A R and Kayabekir A E 2025 Optimisation of fixed supported castellated steel beams. *Int. J. Eng. Technol.* 10: 1–8.

[27] Albayati M A S and Noori A R 2026 Multi-algorithm optimisation and dimensional assessment of steel castellated beams with sinusoidal web openings subjected to static loads. *Asian J. Civ. Eng.* 27: 993–1009.

[28] Beskirli A and Dag I 2023 I-CPA: An improved carnivorous plant algorithm for solar photovoltaic parameter identification problem. *Biomimetics* 8: 569.

[29] Zhou X, Xing J, Gui W, Heidari A A, Cai Z, Chen H and Liang G 2025 Covariance matrix adaptation driven dynamic multi-population colony predation optimiser: insights, qualitative analysis, and constrained engineering optimisation. *Appl. Soft Comput.* 175: 113041.

[30] Egoigwe S V, Chijindu A T, Nwobodo L O, Martha O C, Ozioko F E, Odozo O G and Chidi E U 2025 Comparing multi-control algorithms for complex nonlinear system: an embedded programmable logic control application. *Int. J. Power Electron. Drive Syst.* 16: 212–224.

[31] Mandal D, Ghoshal S P and Bhattacharjee A K 2011 Application of evolutionary optimisation techniques for finding the optimal set of concentric circular antenna array. *Expert Syst. Appl.* 38: 2942–2950.

[32] Kaveh A, Ghazaan M I and Bakhshpoori T 2013 An improved ray optimisation algorithm for design of truss structures. *Period. Polytech. Civ. Eng.* 57: 97–112.

[33] AI S 2025 Collaborative Research: CS2: DANUBE: Formal Methods for Scientific Computing Bridging the Data-Numerics Behaviour Tug-of-War. NSF Award Number 2446083. National Science Foundation.

[34] Zaimoglu E A, Celebi N and Yurtay N 2020 An intelligent feature selection method for finding rough set reducts based on tug of war optimisation algorithm. In: *Intelligent and Fuzzy Techniques in Big Data Analytics and Decision Making: Proceedings of the INFUS 2019 Conference*, Istanbul, Turkey, July 23–25, 2019. pp. 1225–1234. Springer International Publishing.

[35] Kaveh A and Shokohi F 2016 Optimum design of laterally supported castellated beams using tug of war optimisation algorithm. *Struct. Eng. Mech.* 58: 533–553.

[36] Nguyen T, Hoang B, Nguyen G and Nguyen B M 2020 A new workload prediction model using extreme learning machine and enhanced tug of war optimisation. *Procedia Comput. Sci.* 170: 362–369.

[37] Ghelichi M, Goltabar A M, Tavakoli H R and Karamodin A 2021 Neuro-fuzzy active control optimised by tug of war optimisation method for seismically excited benchmark highway bridge. *Numer. Algebra Control Optim.* 11: 333–351.

[38] Albayati M A S 2026 Efficient cost-based design optimisation of castellated beams with circular and hexagonal openings using the grey wolf algorithm. *Fayoum Univ. J. Eng.* 9: 1–13.

[39] Kaveh A and Ilchi Ghazaan M 2020 A new VPS-based algorithm for multi-objective optimisation problems. *Eng. Comput.* 36: 1029–1040.

[40] Almufti S M 2022 Vibrating particles system algorithm performance in solving constrained optimisation problem. *Acad. J. Nawroz Univ.* 10.

[41] Andrade J C, Lobato F S, Neiro S M, Libotte G B and Platt G M 2024 A novel multi-objective optimisation strategy based on vibrating particle system algorithm applied to chemical process design. *Chem. Eng. Res. Des.* 208: 161–183.

[42] Rezazadeh F and Talatahari S 2020 Seismic energy-based design of BRB frames using multi-objective vibrating particles system optimisation. *Structures* 24: 227–239.

[43] Albayati M A S 2026 A hybrid FA–FPA optimization strategy delivering structural, economic and numerical efficiency in cellular beam design. Engineering Computations. Advance online publication. https://doi.org/10.1108/EC-12-2025-1456.

[44] Alhussen A, Alutaibi A I, Sharma S K, Khan A R, Ahmad F and Tejani G G 2025 Early attention-deficit/hyperactivity disorder (ADHD) with NeuroDCT-ICA and rhinofish optimisation (RFO) algorithm based optimised ADHD-Attention. *Net. Sci. Rep.* 15: 6967.

[45] Idoumghar L, Cherin N, Siarry P, Roche R and Miraoui A 2013 Hybrid ICA–PSO algorithm for continuous optimisation. *Appl. Math. Comput.* 219: 11149–11170.

[46] Acharya D P, Panda G and Lakshmi Y V S 2010 Effects of finite register length on fast ICA, bacterial foraging optimisation-based ICA and constrained genetic algorithm-based ICA algorithm. *Digit. Signal Process.* 20: 964–975.

[47] Hosseini-Moghari S M, Morovati R, Moghadas M and Araghinejad S 2015 Optimum operation of reservoir using two evolutionary algorithms: imperialist competitive algorithm (ICA) and cuckoo optimisation algorithm (COA). *Water Resour. Manag.* 29: 3749–3769.

[48] Nguyen T K, Vo T P and Thai H T 2013 Static and free vibration of axially loaded functionally graded beams based on the first-order shear deformation theory. *Compos. Part B Eng.* 55: 147–157.

[49] Chen W R and Chang H 2017 Closed-form solutions for free vibration frequencies of functionally graded Euler-Bernoulli beams. *Mech. Compos. Mater.* 53: 79–98.

[50] Kaveh A and Bakhshpoori T 2019 Metaheuristics: Outlines, MATLAB codes and examples. Springer, Cham, pp 36–65.

Springer Nature or its licensor (e.g. a society or other partner) holds exclusive rights to this article under a publishing agreement with the author(s) or other rightsholder(s); author self-archiving of the accepted manuscript version of this article is solely governed by the terms of such publishing agreement and applicable law.